International Journal of Thermal Sciences 49 (2010) 504–513

Contents lists available at ScienceDirect

International Journal of Thermal Sciences

journal homepage: www.elsevier.com/locate/ijts

Heat transfer enhancement in microchannels with cross-flow synthetic jets

T.T. Chandratilleke*, D. Jagannatha, R. Narayanaswamy

Department of Mechanical Engineering, Curtin University of Technology, GPO Box U1987, Perth WA 6845, Australia

ARTICLE INFO

Article history:
Received 11 November 2008
Received in revised form
12 September 2009
Accepted 14 September 2009
Available online 8 October 2009

Keywords:
Synthetic jet
Microchannel
Electronic cooling
Pulsating jet heat transfer

ABSTRACT

This paper examines the effectiveness of using a pulsating cross-flow fluid jet for thermal enhancement in a microchannel. The proposed technique uses a novel flow pulsing mechanism termed "synthetic jet" that injects into the microchannel a high-frequency fluid jet with a zero-net-mass flow through the jet orifice. The microchannel flow interacted by the pulsed jet is modelled as a two-dimensional finite volume simulation with unsteady Reynolds-averaged Navier–Stokes equations while using the Shear-Stress-Transport (SST) k–ω turbulence model to account for fluid turbulence. For a range of conditions, the special characteristics of this periodically interrupted flow are identified while predicting the associated convective heat transfer rates. Results indicate that the pulsating jet leads to outstanding thermal performance in the microchannel increasing its heat dissipation by about 4.3 times compared to a channel without jet interaction within the tested parametric range. The degree of enhancement is first seen to grow gently and then rather rapidly beyond a certain flow condition to reach a steady value. The proposed strategy has the unique intrinsic ability to generate outstanding degree of thermal enhancement in a microchannel without increasing its flow pressure drop. The technique is envisaged to have application potential in miniature electronic devices where localised cooling is desired over a base heat dissipation load.

1. Introduction

Effective cooling solutions are critical for the design of electronic devices for preventing thermal breakdown and extending working life of semiconductor components. A dramatic increase in internal heat generation in modern microelectronic devices has exacerbated the cooling requirements in recent years. In the face of this, the conventional cooling methods are rapidly becoming inadequate for dissipating intense heat loads often encountered in new microprocessors. The microelectronic industry signals an urgent need to develop practical and effective cooling methods that surpass current thresholds of thermal performance. Microchannel heat sinks have become the frontier technology in this respect and show well recognised potential for meeting high heat dissipation needs.

A recent update by International Technology Roadmap for Semiconductors (ITRS) in 2008 has predicted a dramatic increase in the number of components integrated into a single unit, as illustrated in Fig. 1. Exponential growth in applications over the past decade has motivated and intensified research to discover novel techniques to further enhance heat transfer capabilities of microchannels towards meeting future demands.

Microchannel behaviour is relatively well understood through established numerical modelling methods and experimentation. Conducting numerical and experimental studies with rectangular microchannels up to 534 μm in size, Lee et al. [1] have shown that the conventional Navier–Stokes equations do accurately predict microchannel characteristics with just 5 percent deviation between numerical and experimental data. Among many others, Qu and Mudawar [2] have also drawn similar conclusions on the use of conventional equations for microchannel analysis. Lee and Garimella [3] have examined the effects of microchannel channel aspect ratio in thermally developing laminar flow. Using a three-dimensional numerical model, they developed a generalised correlation for both local and average Nusselt number in terms of microchannel aspect ratio. Having validated against the experimental data for both mini and micro-scale ducts, this correlation is universally recognised for its applicability. The present work considers an extensive computational fluid dynamics model for microchannel analysis in line with the current state of numerical modelling, such as the simulation work of Fedorov and Viskanta [4].

The primary focus of microchannel research is to predict and validate thermal performance. Much less attention has been directed for developing effective thermal enhancement strategies for microscale channels. Reviewing published literature on single-phase

* Corresponding author. Tel.: +61 8 9266 7047.
E-mail address: t.chandratilleke@curtin.edu.au (T.T. Chandratilleke).

1290-0729/$ – see front matter
doi:10.1016/j.ijthermalsci.2009.09.004

Nomenclature

A	diaphragm amplitude, mm
d_c	cavity width, mm
d_o	orifice width, mm
D	channel width, mm
f	diaphragm frequency, kHz
h	local convective heat transfer coefficient, W/m^2 K
h_c	cavity height, mm
h_o	orifice height, mm
H	channel height, mm
L	heater width, mm
k	thermal conductivity of air, W/m K
L_s	stroke length, m
Nu	local Nusselt number based on heater length, (hL/k)
Re_c	Reynolds number, $(U_c d_o/\nu)$
S	Stokes number, $(\sqrt{\omega d_o^2/\nu})$
t	time, s
T	time period, $(1/f)$, s
T_b	bulk temperature, K
T_w	wall temperature, K
U_c	characteristic velocity, m/s
u_o	velocity through orifice, m/s
V_i	microchannel inlet velocity, m/s

Greek symbols

ρ	density of air, kg/m^3
μ	dynamic viscosity of air, kg/ms
ω	angular velocity, rad/s
ν	kinematic viscosity of air, m^2/s

micro and minichannel heat transfer, Steinke and Kandlikar [5] have cited that the use of internal fins in microchannels is a very promising passive enhancement option although the increased pressure drop would be a design concern. Narayanaswamy et al. [6] report a comprehensive treatment on such internal fins and possibilities for thermal optimisation.

While passive enhancement techniques have conceivable application potential, active methods may prove to be more thermally effective and relevant for future cooling needs, especially if the thermal enhancement is possible without incurring a penalty through increased pressure drop. As discussed in the sections below, the microchannel flow interrupted by a pulsating fluid jet is envisaged to be an option of this nature.

The present study examines the performance of a new active enhancement method that can be integrated into microchannel heat sinks. As schematically shown in Fig. 2, the proposed method adopts a pulsating jet mechanism called a "synthetic jet" that interacts with the flow through the microchannel whereby outstanding thermal characteristics are achieved without incurring adverse pressure drop penalties.

The synthetic jet mechanism mounted on the microchannel comprises an oscillating diaphragm that moves back and forth at frequency (f) forcing fluid flow through a small orifice. In its inward motion, the diaphragm imparts a high-speed jet into the microchannel creating a pair of counter-rotating vortices in the surrounding fluid. When retreating, it draws fluid back into the cavity. The fluid ejected through the orifice and the vortices

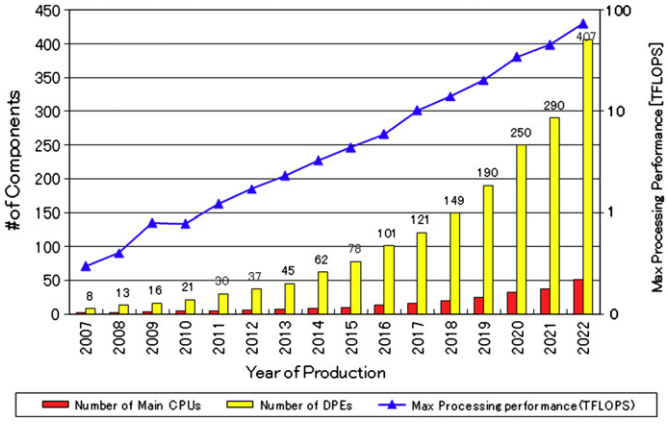

Fig. 1. Consumer stationary design complexity trends-source ITRS 2008.

periodically interrupt and interact in cross-flow manner with the microchannel fluid flow. Over one diaphragm cycle, the jet discharges an intense net outflow of fluid momentum into the microchannel while the net mass delivered through the orifice is zero. Therefore, this jet mechanism is known as a "synthetic jet" or Zero-Net-Mass-Flux jet.

Synthetic jets have been primarily studied in the context of pulsating jet actuators impinging on submerged surfaces in quiescent fluid media without any cross-flow interactions. Such studies indicate outstanding thermal characteristics for localised cooling with synthetic jets. Significant examples of those are by Campbell et al. [7] who have demonstrated that synthetic air micro jets were effective cooling arrangements for laptop processors while Mahalingam et al. [8,9] illustrated the effectiveness of synthetic jets for high power electronic cooling by developing an integrated active heat sink based on this mechanism. Gillespie et al. [10] provide the results of an experimental investigation of a rectangular synthetic jet impinging on an unconfined heated plate exposed to the ambient where characteristics of the jet and plots of Nusselt numbers are available. Pavlova and Amitay [11] have conducted experimental studies on impinging synthetic jets for constant heat flux surface cooling and compared its performance with a jet having no velocity fluctuations known as steady or continuous jet. They concluded that for the same Reynolds number, synthetic jets provide three times more effective cooling than the corresponding continuous jets.

Aiming at flow control applications, the aerospace research studies have examined synthetic jets interacting with fluid cross-flow. However, the impact of these interactions on thermal flow characteristics has rarely been investigated for heat transfer applications where very little such knowledge currently exists. Among few reported studies addressing this shortfall, Jabbal and Zhong [12] experimentally examined a case of synthetic jet discharged from an orifice on a heated surface into a low-Reynolds number laminar flow. For this non-surface impinging jet flow, they mapped out the thermal footprint of the jet flowing over the heated surface using liquid crystal thermography. However, the investigation did not assess the impact of this synthetic jet on thermal performance.

Utturkar et al. [13] experimentally studied synthetic jet acting parallel to the flow within a duct. The synthetic jet was placed at the surface of a heated duct wall and aligned with the bulk flow such that the jet assisted the bulk flow. In a 100 mm square channel with a 30 mm synthetic jet, they obtained a 5.5 times enhancement for a bulk flow velocity 1 m/s. This enhancement reduced to approximately 3 times when the bulk velocity was increased to of

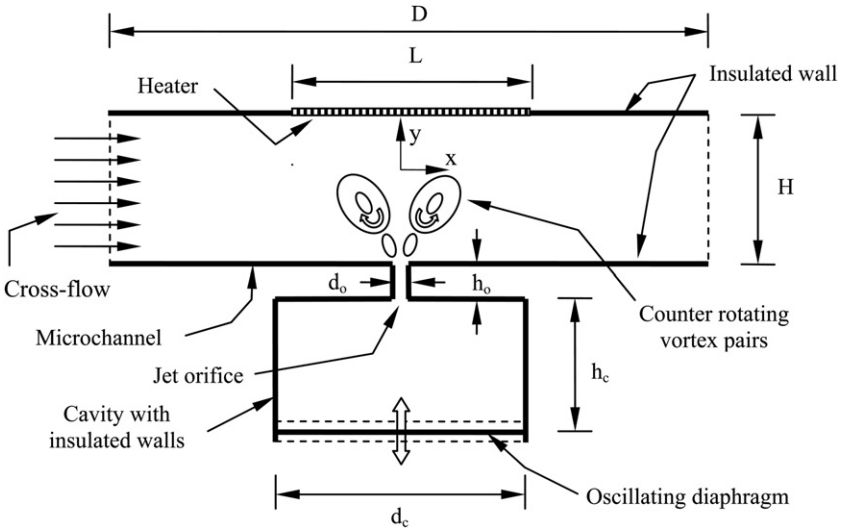

Fig. 2. Schematic diagram of synthetic jet mounted on microchannel in cross-flow configuration.

2.0 m/s. Their restricted numerical simulation matched reasonably well with only one test condition.

Go and Mongia [14] experimentally studied the effect of introducing a synthetic jet into a low speed duct flow to emulate the confined flow within in a typical notebook. The interaction of these two flows was studied using particle image velocimetry (PIV) and measurements on the heated duct wall. They found that the synthetic jet tends to retard or block the duct flow while a 25 percent increase in thermal performance was observed.

Numerical studies on thermal performance of synthetic jet with cross-flow interaction are also very limited in published literature. Such significant work is presented by Timchenko et al. [15] who investigated the use of a synthetic jet induced by a vibrating diaphragm to enhance the heat transfer in a 200 μm microchannel. Their two-dimensional (2-D) transient simulation considered the jet acting in cross-flow to the bulk flow in the channel with the diaphragm assumed to execute a parabolic motion. They observed a 64 percent improvement in cooling at the impinging wall for the flow conditions used. Despite the recognised significance of flow turbulence in synthetic jet flows, their analysis however did not include an appropriate turbulence model in the simulation.

In a recent study, Erbas and Baysal [16] conducted computational work of a synthetic jet actuator in a two-dimensional channel to assess its thermal effectiveness on a heated surface protruding into the fluid as a step. They varied the number of actuators, placement and phasing of the membrane concluding that the heat transfer rate would increase with the number of jets, appropriate jet spacing, the use of nozzle-type orifice geometry and 180° out of phase jet operation. However, the investigation did not examine the influence of cross-flow on the thermal performance.

The present study examines a novel thermal enhancement strategy for micro-scale heat transfer applications by combining the benefits of highly favourable synthetic jet characteristics and the proven effectiveness of microchannel flows. This hybrid arrangement is envisaged to deliver excellent thermal performance for microchannel heat sinks without the need for additional fluid circuits and large fluid velocities that invariably increase pressure drop. The published literature reports a very few numerical analyses akin to highly interactive combined synthetic jet and microchannel flows considered in this paper while very limited applicable experimental work is available for comparison.

2. Numerical model

2.1. Governing equations

This study investigates the heat transfer characteristics of low-Reynolds number turbulent synthetic jets operating in a confined region while interacting with microchannel flow. Applicable governing equations for the analysis are the Navier–Stokes equations, the continuity equation and the energy equation subject to applied boundary conditions. In this, the equation of continuity is written as:

$$\frac{\partial u}{\partial x}+\frac{\partial v}{\partial y}=0 \tag{1}$$

the momentum equations are expressed as:

$$x\text{-momentum}\quad \frac{\partial u}{\partial t}+u\frac{\partial u}{\partial x}+v\frac{\partial u}{\partial y}=-\frac{\partial p}{\partial x}+\mu\left(\frac{\partial^2 u}{\partial x^2}+\frac{\partial^2 u}{\partial y^2}\right) \tag{2}$$

$$y\text{-momentum}\quad \frac{\partial v}{\partial t}+u\frac{\partial v}{\partial x}+v\frac{\partial v}{\partial y}=-\frac{\partial p}{\partial y}+\mu\left(\frac{\partial^2 v}{\partial x^2}+\frac{\partial^2 v}{\partial y^2}\right) \tag{3}$$

and the energy equation and its associated expressions are written as:

$$\frac{\partial}{\partial t}(\rho E)=-\nabla\cdot(U(\rho E+p))+k\nabla^2 T-(\tau:\nabla U)-\nabla\cdot\left(\sum_k H_k J_k\right)+S_h \tag{4}$$

where, the internal energy E is calculated from,

$$E=H-\frac{p}{\rho}+\frac{U^2}{2} \tag{5}$$

while the specific enthalpy H is obtained from,

$$H=\sum_k x_k H_k \tag{6}$$

For an ideal gas, E and H can be expressed as,

$$E=C_V(T-T_o) \tag{7}$$

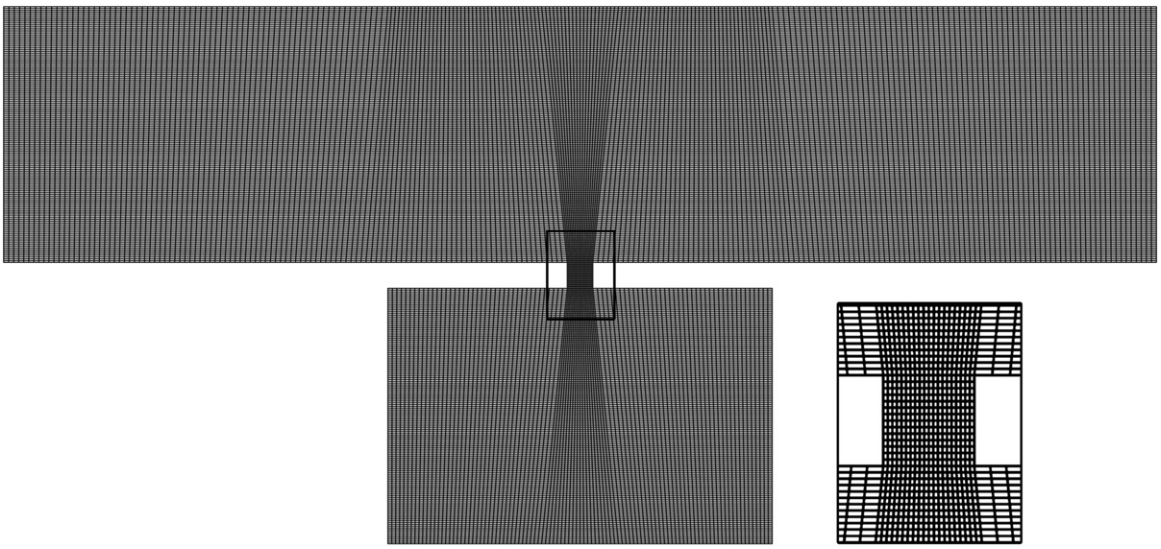

Fig. 3. Computational grid for solution domain [inset shows enlarged view of the marked region].

and

$$H_k = C_{pk}(T - T_o) \tag{8}$$

The local Nusselt number Nu (x,t) wherein the local wall heat transfer coefficient h is embedded, describes the convective heat transfer between the heated surface and the synthetic jet flow. Using orifice width d_o as the characteristic length, this is defined as

$$Nu(x,t) = \frac{hd_o}{k_f} = \frac{\partial T}{\partial y}\frac{d_o}{\Delta T} \tag{9}$$

The Nusselt number is evaluated from the local surface normal temperature gradient, $(\partial T)/(\partial y)$ and the temperature difference $\Delta T = (T_w - T_b)$ where T_w is the local wall temperature and T_b is the average bulk fluid temperature the in the fluid domain.

2.2. Solution domain and boundary conditions

Similar to Fugal and Smith [17] and Wang et al. [18], the present study uses a numerical model developed on the computational fluid dynamics software FLUENT. A structured mesh was developed for the solution domain shown in Fig. 3 using the mesh generation facility GAMBIT. In capturing intricate details of the jet formation and flow separation, the grid density in the vicinity of the orifice was refined to have 14 grid cells in the axial direction and 20 in the transverse direction.

As illustrated by Utturkar et al. [19], the vortex formation in synthetic jet is governed by the non-dimensional groups Reynolds number (Re) and Stokes number (S), and occurs under the parametric condition of $Re/S^2 > K$, where the constant $K \approx 1$ for two-dimensional jets and 0.16 for axi-symmetric synthetic jets. By due consideration of this requirement, the following dimensions were used in the analysis: orifice width $d_o = 50$ μm, orifice length $h_o = 50$ μm, channel height $H = 500$ μm, channel length $D = 2250$ μm, heater length $L = 750$ μm, cavity width $d_c = 750$ μm and cavity height $h_c = 500$ μm. This dimensional selection was checked and confirmed for its compliance with the continuum mechanics for the scale of the attempted problem using Knudsen number Kn, which is the ratio of the molecular free path length to representative length.

Adiabatic conditions were applied at all microchannel walls, the cavity walls and the diaphragm. The heater surface was maintained at an isothermal temperature of 360 K. The (left) flow inlet to the microchannel was treated as a known constant velocity boundary while the (right) flow outlet was treated as pressure outlet boundary. It was assumed that the working fluid air is incompressible and has an inlet temperature of 300 K with constant thermodynamic properties under standard atmospheric conditions.

Arising from small geometrical length scales, synthetic jets generally tend to have small operating Reynolds numbers making flow turbulence seemingly unimportant. However, the oscillating nature of the flow may give rise to intense localised perturbations. In handling the wide flow variations, the Shear-Stress-Transport (SST) k–ω turbulence model was invoked in the model to provide an accurate representation of the near-wall region of wall-bounded turbulent flows. Since the length scale in the present simulation is small, a turbulence intensity of 3 percent was applied at the outlets. The $y+$ and y^* value in the wall region were found to be approximately 1, confirming that the near-wall mesh resolution is in the laminar sublayer.

2.3. Initial conditions and solution methodology

The initial ($t = 0$) position of the diaphragm was taken to be at the bottom of the cavity. A special User Defined Function (UDF) incorporating dynamic-layering technique [20] was formulated and combined with the FLUENT solver to describe the periodic diaphragm movement. For this, the diaphragm displacement was expressed as $y = A\sin(\omega t)$, where A is the diaphragm amplitude, ω is the angular frequency and t is time.

A segregated solution method with implicit solver formulation in FLUENT was used as the numerical algorithm while the second-order discretisation schemes were employed for density, momentum, pressure, kinetic energy, specific dissipation rate and energy. The Pressure-Implicit with Splitting of Operators (PISO)

Table 1
Parametric range for numerical simulation.

Parameter	Range
Microchannel inlet velocity, V_i (m/s)	0, 0.5, 1.0, 2.0
Diaphragm frequency, f (kHz)	10
Diaphragm amplitude, A (μm)	0, 25, 50, 75, 100
Jet Reynolds number, Re_c	15, 30, 46, 62
Distance from orifice to heated wall, H/d_o	10

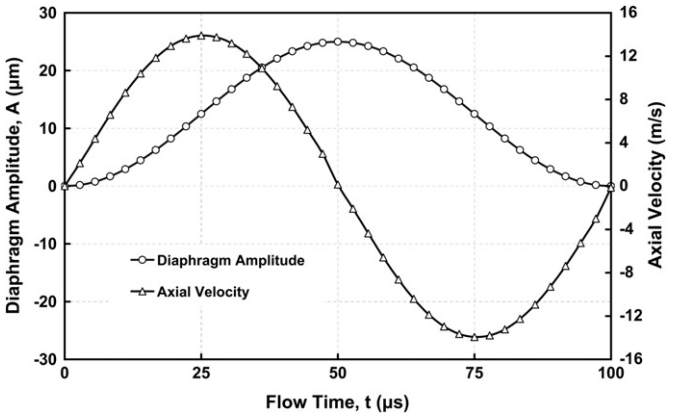

Fig. 4. Diaphragm displacement and jet velocity during one complete cycle ($f = 10$ kHz and $A = 25$ μm).

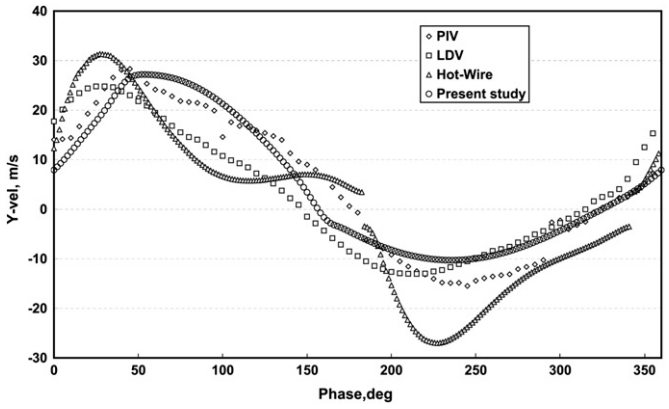

Fig. 5. Comparison of predicted axial/y-velocity of present work with the (PIV, LDV, Hot-wire) experimental data of Yao et al. [22] at 0.1 mm from the orifice exit plane ($f = 444.7$ Hz, $A = 1.25$ mm).

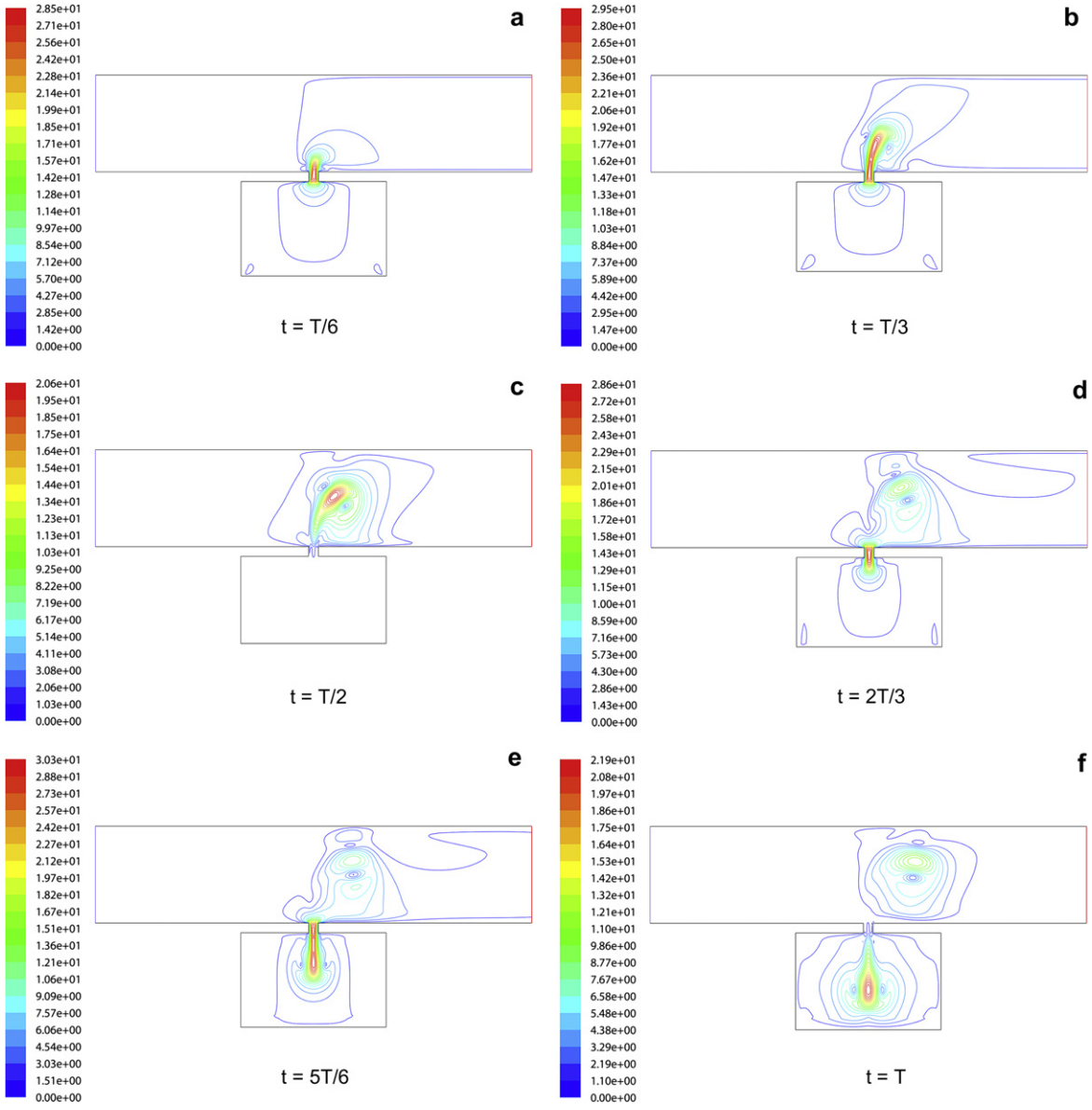

Fig. 6. (a–f): Time-lapsed velocity contours for one cycle $V_i = 0.5$ m/s, $A = 50$ μm and $f = 10$ kHz.

scheme was used for pressure-velocity coupling. The bulk temperature of air at every time step was calculated using a UDF while the updated bulk temperature was fed back to the simulation for calculating local heat transfer coefficient and Nusselt number.

The jet Reynolds number (Re_c) was calculated based on the jet characteristic velocity U_c, which is defined by Smith and Glezer [21] as,

$$U_c = L_s f = \frac{1}{T}\int_0^{T/2} u_o(t)\mathrm{d}t \tag{10}$$

where $u_o(t)$ is the jet velocity at the orifice discharge plane, ½T is the jet discharge time or half period of diaphragm motion, and L_s is the stroke length (defined as the discharged fluid length through orifice during the upward diaphragm stroke).

With these imposed conditions, the unsteady, Reynolds-averaged Navier–Stokes equations within the solution domain were solved along with the energy equation for a range of operating conditions, which are given in Table 1.

For an operating frequency of 10 kHz and diaphragm amplitude of 25 μm, Fig. 4 illustrates the diaphragm displacement and the jet discharge velocity over one full cycle completed in 0.1 ms. The simulation was carried out using 720 time steps per cycle wherein 20 sub-iterations were performed within each time step. At each time step of a cycle, the internal iterations were continued until the residuals of mass, momentum, turbulence parameters (k and ω) were reduced below 10^{-3} and energy residuals were reduced below 10^{-6}, which is the convergence criterion for the computation. Data were extracted at every twentieth time step giving 36 data points per cycle. It was observed that 10 diaphragm cycles would be sufficient to achieve quasi-steady operating conditions in this microchannel flow geometry.

The grid dependency of results was tested by observing the changes to time-averaged velocity fields in the solution domain for varied grid sizes. In view of the moving mesh integrity and CPU time, the most appropriate grid size was found to be 48 072 cells for a five percent tolerance between successive grid selections. To increase accuracy, a 2-D-double precision solver was used to solve the governing equations for heat and fluid flow.

3. Results and discussion

3.1. Model validation

The model validation for the present simulation was carried out by developing a separate synthetic jet model by altering the micro-scale domain dimensions to match the published work involving mini-scale geometries of Yao et al. [22]. These results were extensively incorporated in NASA Langley Research Centre Workshop (CFDVAL2004) [23] in assessing suitability of turbulence models for synthetic jet flows. The results of the workshop indicated that the turbulence model selected significantly affected the results and Shear-Stress-Transport (SST) k–ω turbulence model works best among the URANS models.

To match the NASA workshop study case, the model chosen had an orifice diameter of d_o = 1.27 mm, diaphragm amplitude

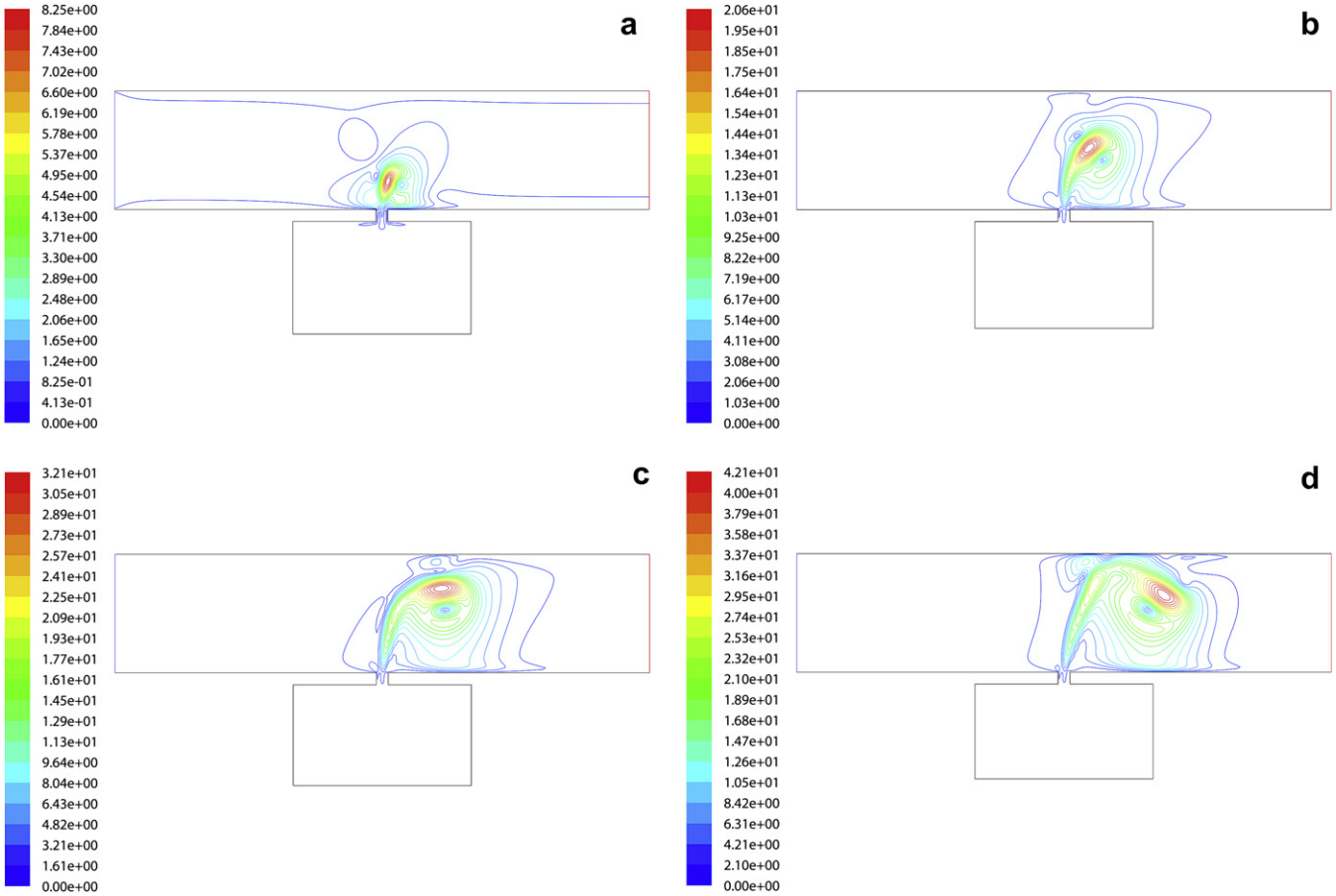

Fig. 7. (a–d): Velocity contours at peak diaphragm displacement (t = ½T) for f = 10 kHz, V_i = 0.5 m/s and A = 25, 50, 75 and 100 μm respectively.

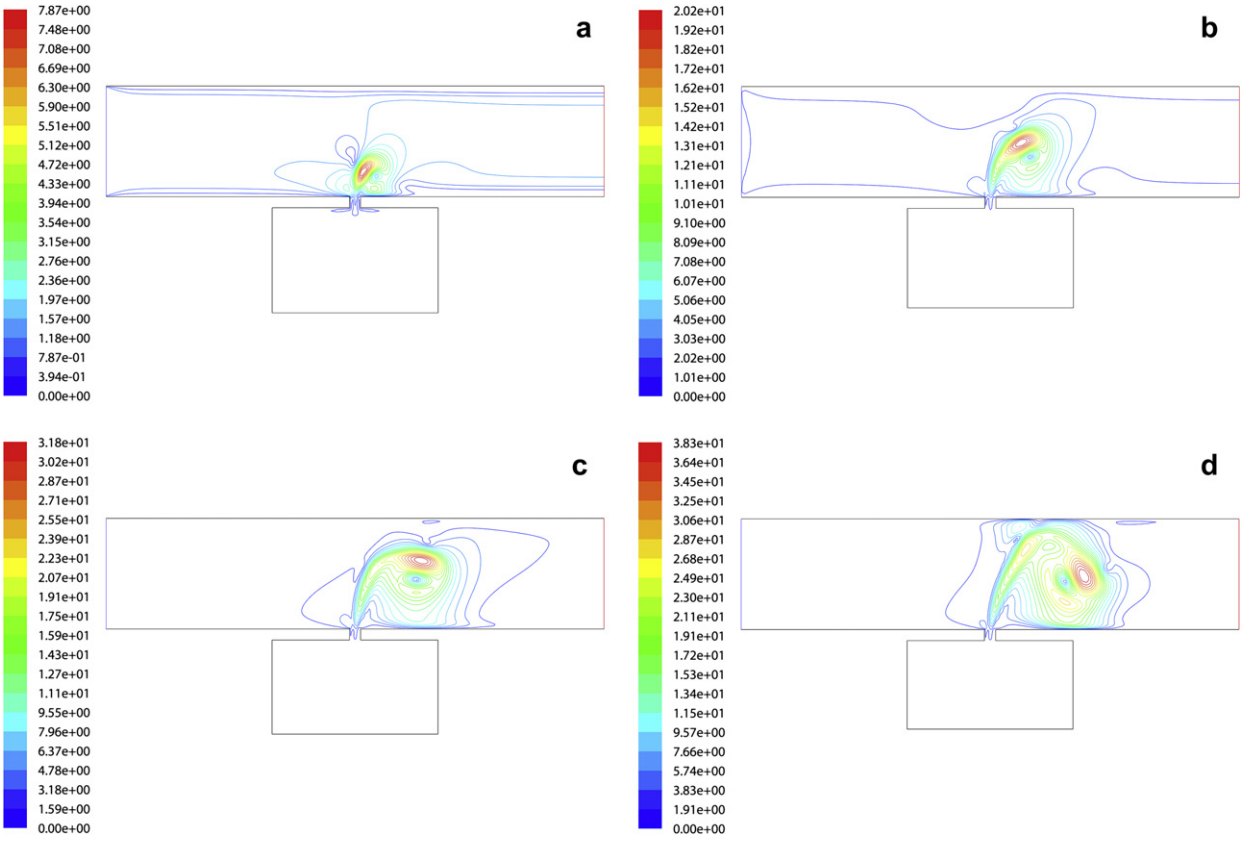

Fig. 8. (a–d): Velocity contours at peak diaphragm displacement ($t = ½T$) for $f = 10$ kHz, $V_i = 1$ m/s and $A = 25$, 50, 75 and 100 μm respectively.

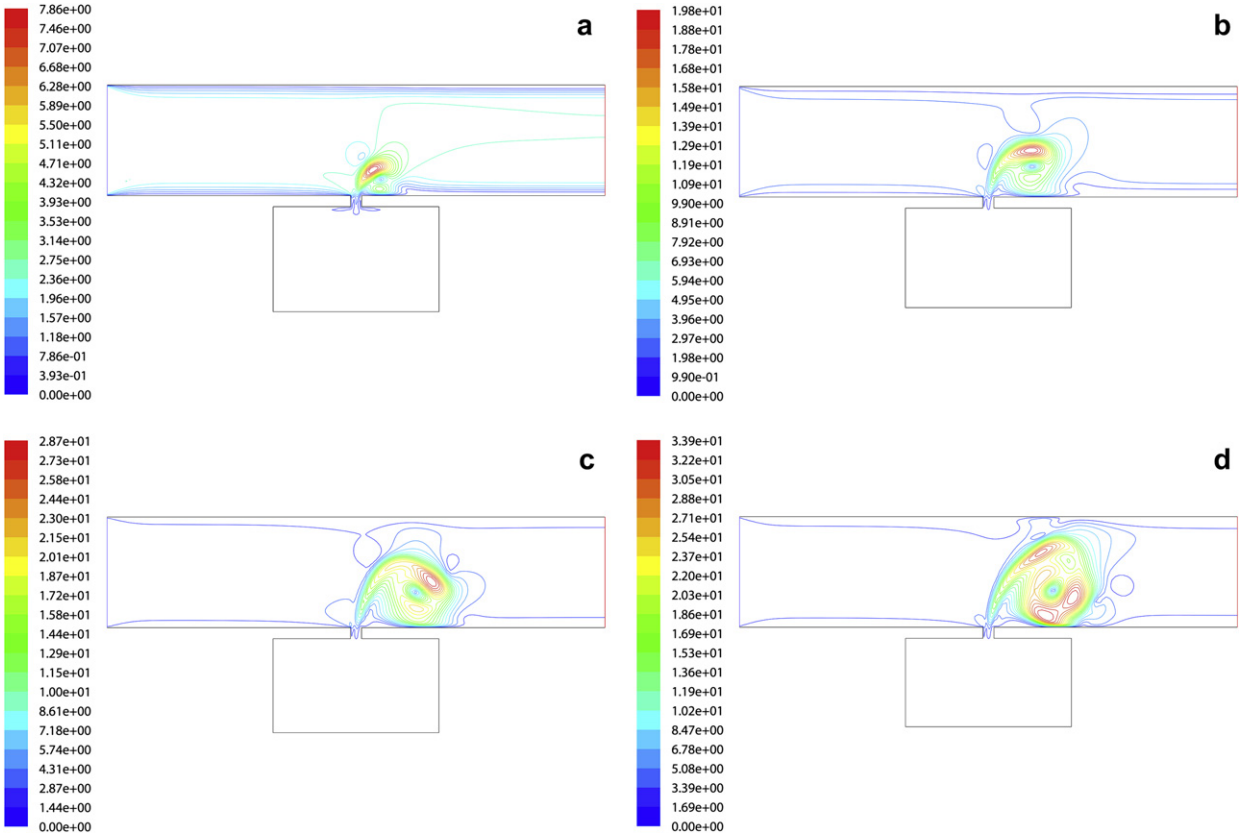

Fig. 9. (a–d): Velocity contours at peak diaphragm displacement ($t = ½T$) for $f = 10$ kHz, $V_i = 2$ m/s and $A = 25$, 50, 75 and 100 μm respectively.

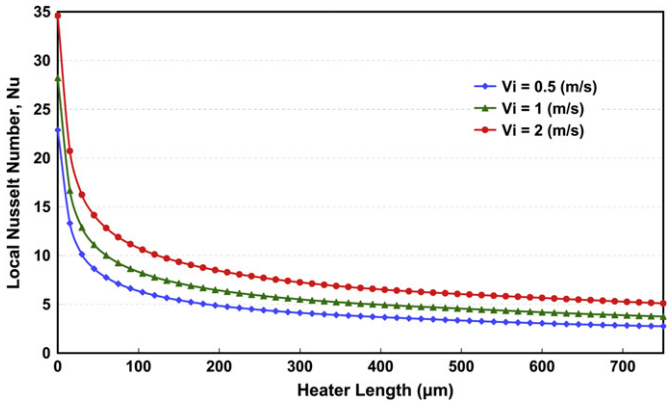

Fig. 10. Variation of local Nusselt number at the heated wall for different microchannel inlet velocities.

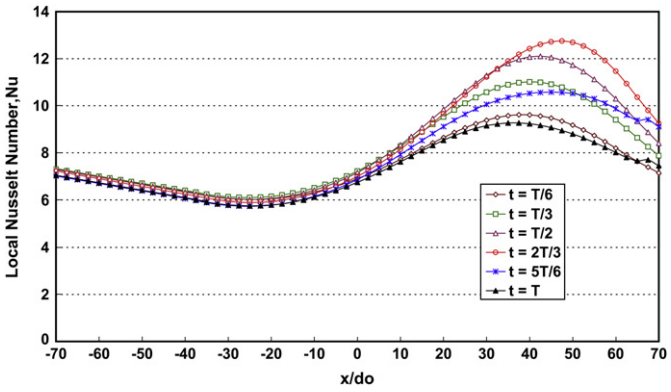

Fig. 12. Distribution of local Nusselt number at the heated wall over one cycle $f = 10$ kHz, $A = 50$ μm and $V_i = 1$ m/s.

$A = 1.25$ mm and diaphragm frequency 444.7 Hz. As depicted in Fig. 5, the predicted axial (y-velocity) was compared with the experimental jet velocities measured by Yao et al. [22] using the techniques of Particle Image Velocimetry (PIV), Hot wire anemometry and Laser Doppler Velocimetry (LDV). It is clearly seen that the present simulation agrees very well with the experimental data validating the model and its accuracy. The details of this validation are further discussed in Jagannatha et al. [24].

3.2. Velocity and fluid flow characteristics

Fig. 6a–f shows typical time-lapsed velocity contours within the solution domain for the conditions of diaphragm amplitude 50 μm, microchannel inlet velocity 0.5 m/s and diaphragm frequency 10 kHz. The figure illustrates the nature of cross-flow interaction occurring in the microchannel due to the pulsating fluid synthetic jet during one cycle of operation.

During the diaphragm upward motion, a high-velocity fluid jet is discharged through the cavity orifice into the microchannel flow. Determined by diaphragm amplitude, sufficiently strong jet momentum enables the jet to penetrate the microchannel flow to reach the heated (upper) wall within the time up to $t = ½T$ at peak diaphragm displacement.

In Fig. 6c, the formation of synthetic jet vortices is clearly visible during this initial phase of sequence. The asymmetry of the flow pattern is due to the cross-flow drag imparted by the microchannel fluid stream.

For $t > ½T$, the diaphragm retreats from its peak displacement to complete the cycle. During this final phase, the synthetic jet mechanism draws fluid back into the cavity. Meanwhile, the synthetic jet vortices formed previously are dragged downstream by the microchannel flow.

The synthetic jet action periodically interrupts the microchannel flow and breaks up the developing thermal and hydrodynamic boundary layers at the heated top wall. This cross-flow interaction creates steep velocity and temperature gradients at the heated surface as long as jet impingement occurs. This pulsating flow mechanism therefore leads to improved thermal characteristics in the synthetic jet-mounted microchannel arrangement.

Relative strengths of the synthetic jet and the microchannel flow drag determine the extent of cross-flow interference and the boundary layer disruption at the heated wall. This is illustrated in Figs. 7a–d, 8a–d and 9a–d for microchannel velocities of 0.5 m/s, 1.0 m/s and 2.0 m/s respectively. It is clearly evident that the increased microchannel flow causes the jet to be swayed downstream. This impedes the jet's ability to penetrate through the boundary layer to reach the heated wall to bring about favourable thermal characteristics.

3.3. Thermal characteristics and heat transfer enhancement

In order to obtain a baseline data to determine the degree of thermal enhancement, the synthetic jet was switched off and heat transfer measurements were made with only the microchannel inlet flow. Fig. 10 depicts the predicted distribution of local Nusselt numbers over the heated wall for different microchannel inlet velocities. The behaviour is similar to flow over a flat plate, which is noted to decay from its peak value at the leading edge of the heated wall.

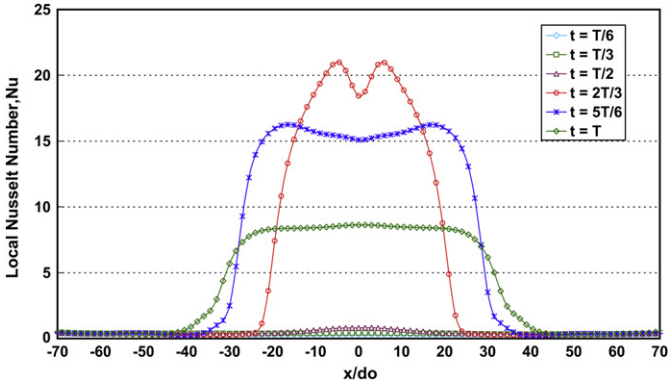

Fig. 11. Distribution of local Nusselt number at the heated wall over one cycle $f = 10$ kHz, $A = 50$ μm and $V_i = 0$ m/s.

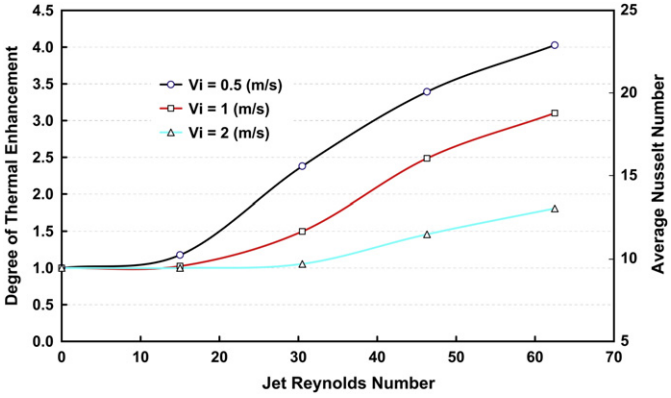

Fig. 13. Degree of thermal enhancement and Nusselt number due to synthetic jet mechanism.

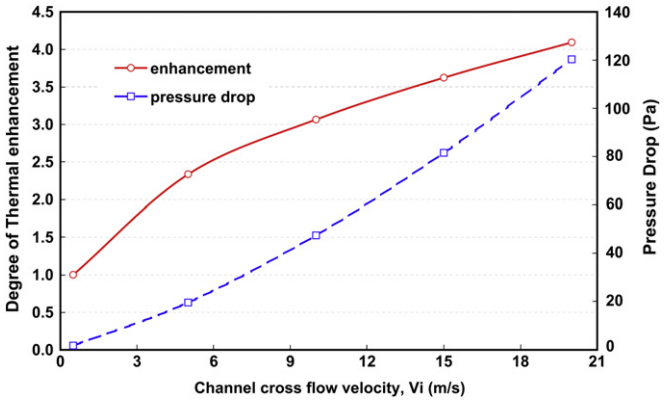

Fig. 14. Thermal enhancement and pressure drop of microchannel flow without synthetic jet mechanism.

For a typical case with stagnant fluid ($V_i = 0$ m/s) in the microchannel, Fig. 11 shows the distribution of local Nusselt numbers over the heated wall for several time steps during one cycle of operation. It indicates that initially, the Nusselt number remains very low for $0 < t < ½T$. During this period, the synthetic jet vortices have yet to impinge on the heated surface. The Nusselt number very rapidly increases to about 23 for $t = 2T/3$ when the vortices begin to interact with the heated surface. A gentle decline in the Nusselt number is then noticed for $t > 2T/3$.

Fig. 12 shows a typical distribution of local Nusselt numbers at the heated wall over one cycle for the case of fluid flowing ($V_i = 1$ m/s) in the microchannel. It is noticed that the distribution now shifted downstream and the peak value of the Nusselt number is reduced to about 13. This is because the increased microchannel flow interacts with the impinging jet and drags it with the flow, as depicted in Figs. 7–9. Thus, the velocity and temperature gradients at the heated wall are reduced along with the heat transfer rates.

Fig. 13 depicts the degree of thermal enhancement achieved by the introduction of a cross-flow pulsating synthetic jet for selected microchannel flow velocities. In this, the thermal performance of microchannel flow without the cross-flow jet mechanism is taken as the datum, which represents the value of 1.0 at zero jet Reynolds number. For the tested range of diaphragm amplitude, jet frequency and microchannel velocity, the synthetic jet mechanism delivers about 4.3 times thermal enhancement in the microchannel compared to a channel without pulsating jet. Because of the nature of synthetic jet mechanism, this degree of thermal enhancement is realised without introducing additional net mass flow into the microchannel or requiring additional fluid circuits, which is recognised as a major operational benefit.

Fig. 13 further shows that the higher microchannel velocity impairs thermal enhancement level. As explained previously with reference to Figs. 7–9, the reason for this reduced performance is because the drag of microchannel flow swaying the synthetic jet downstream preventing jet impingement on the heated surface. As the jet Reynolds number (or jet velocity or diaphragm amplitude) is increased for a fixed microchannel velocity, the degree of thermal enhancement suddenly increases when the jet is able to penetrate and reach the heated surface. A typical case for this illustrated by the flow pattern depicted in Fig. 7c and d for a microchannel velocity of 0.5 m/s. In Fig. 13, the corresponding situation is shown by the onset of sharp elevation in thermal enhancement gradient at a jet Reynolds number of approximately 15. As the microchannel velocity is increased, this point of rapid growth tends to shift towards higher values of jet Reynolds number.

Fig. 14 shows the thermal performance and the pressure drop of microchannel flow without synthetic jet mechanism. It is seen for example that, to obtain 4.3 times thermal enhancement possible with the hybrid microchannel having flow velocity of 0.5 m/s, a channel without the pulsed jet will need 40 times velocity increase. Such a channel will have very adverse 70-fold increase in flow pressure drop. This clearly demonstrates the significant potential for thermal enhancement in microchannels with this hybrid arrangement and its operational benefits as an enhancement technique.

4. Conclusions

Through a numerical simulation, a novel thermal enhancement strategy for microchannels has been successfully demonstrated. The proposed technique incorporates a pulsating fluid jet generated by a special mechanism called “Synthetic Jet” that injects net positive fluid momentum with zero averaged jet mass flow into the microchannel. The pulsing jet interacts with the microchannel flow and gives rise to excellent thermal characteristics at the heated wall. In the tested range, this unique technique is capable of delivering a 4.3 fold increase in microchannel heat transfer without higher flow rate or pressure drop, which is the key operational attribute in this method that sets it apart from other thermal enhancement strategies. Also, this arrangement does not require the deployment of additional fluid flow circuits to achieve such high heat transfer rates.

References

[1] P.S. Lee, S.V. Garimella, D. Liu, Investigation of heat transfer in rectangular microchannels. International Journal of Heat and Mass Transfer 48 (9) (2005) 1688–1704.
[2] W. Qu, I. Mudawar, Experimental and numerical study of pressure drop and heat transfer in a single phase microchannel heat sink. International Journal of Heat and Mass Transfer 45 (2) (2002) 2549–2565.
[3] P.S. Lee, S.V. Garimella, Thermally developing flow and heat transfer in rectangular mircochannels. International Journal of Heat and Mass Transfer 49 (17) (2006) 3060–3067.
[4] A.G. Fedorov, R. Viskanta, Three dimensional conjugate heat transfer in the microchannel heat sink for electronic packaging. International Journal of Heat and Mass Transfer 43 (3) (2000) 399–415.
[5] M.E. Steinke, S.G. Kandlikar, Single Phase Heat Transfer Enhancement Technique in Microchannel and Minichannel Flows, International conference of Microchannel and Minichannels, 2004, pp. 141–148, ICMM 2004-2328.
[6] R. Narayanaswamy, T.T. Chandratilleke, J.L. Foong, Laminar convective heat transfer in a microchannel with internal fins, in: Proceedings of the Sixth International ASME Conference on Nanochannels, Microchannels, and Minichannels, ICNMM 2008–62044, 2008.
[7] J.S. Campbell, W.Z. Black, A. Glezer, Thermal Management of a Laptop Computer with Synthetic Air Microjets, InterSociety Conference on Thermal Phenomena. IEEE, 1998, pp. 43–50.
[8] R. Mahalingam, A. Glezer, Air Cooled Heat Sinks Integrated with Synthetic Jets, in InterSociety Conference on Thermal Phenomena. IEEE, 2002, pp. 285–291.
[9] R. Mahalingam, N. Rumigny, Thermal management using synthetic jet ejectors. IEEE 27 (3) (2004) 439–444.
[10] M.B. Gillespie, W.Z. Black, C. Rinehart, A. Glezer, Local convective heat transfer from a constant heat flux flat plate cooled by synthetic air jets. Journal of Heat Transfer 128 (2006) 990–1000.
[11] A. Pavlova, M. Amitay, electronic cooling using synthetic jet impingement. Journal of Heat Transfer 128 (9) (2006) 897–907.
[12] M. Jabbal, S. Zhong, The near wall effect of synthetic jets in a boundary layer. International Journal of Heat and Fluid Flow 29 (2007) 119–130.
[13] Y. Utturkar, M. Arik, M. Gursoy, Assessment of cooling enhancement of synthetic jet in conjunction with forced convection, in: Proceedings of IMECE2007, Seattle, USA, November 11–15, 2007
[14] D.B. Go, R.K. Mongia, Experimental Studies on Synthetic Jet Cooling Enhancement for Portable Platforms. IEEE, 2008, pp. 528–536.
[15] V. Timchenko, J. Reizes, E. Leonardi, A numerical study of enhanced microchannel cooling using a synthetic jet actuator, in: Proceedings of the 15th Australasian Fluid Mechanics Conference, Sydney, Australia, 2004
[16] N. Erbas, O. Baysal, Micron-level actuators for thermal management of microelectronic devices. Heat Transfer Engineering 30 (1–2) (2009) 138–147.
[17] S.R. Fugal, B.L. Smith, A Numerical Study of 2-D Synthetic Jet Formation, in 2004 ASME Heat Transfer/Fluids Engineering Summer Conference. ASME, Charlotte, USA, 2004, pp. 1–6.

[18] Y. Wang, G. Yuan, S.A. Bidstrup, Large eddy simulation (LES) for synthetic jet thermal management. International Journal of Heat and Mass Transfer 49 (13–14) (2006) 2173–2179.
[19] Y. Utturkar, R. Holman, R. Mittal, B.L. Smith, L. Cattafesta, Formation criterion for synthetic jets. AIAA 43 (10) (2005) 2110–2116.
[20] FLUENT User Guide Manual 6.2.16, 2004.
[21] B.L. Smith, A. Glezer, The formation and evolution of synthetic jets. Physics of Fluids 10 (September) (1998) 2281–2297.
[22] C.S. Yao, F.J. Chen, D. Neuhart, Synthetic jet flowfield database for computational fluid dynamics validation. AIAA Journal 44 (12) (2006) 3153–3157.
[23] Langley Research Centre Workshop on CFD Validation of Synthetic Jets and Turbulent Separation Control (CFDVAL2004), Williamsburg, Virginia, 2004.
[24] D. Jagannatha, R. Narayanaswamy, T.T. Chandratilleke, Analysis of a synthetic jet-based electronic cooling module. Numerical Heat Transfer, Part A: Applications 56 (3) (2009) 211–229.